Korean J. Chem. Eng., 39(3), 760-774 (2022)
DOI: 10.1007/s11814-021-0931-0

pISSN: 0256-1115
eISSN: 1975-7220

Isolation, characterization and methylene blue adsorption: Application of cellulose from olive sawdust

Fatma. Njeh*, Morched. Hamza*, Ines. Bouaziz*, Ridha. Abdelhedi*, and Makki. Abdelmouleh,†**

*Laboratory of Electrochemistry and Environment (LEE), Sfax National Engineering School (ENIS) BPW, 3038 Sfax, University of Sfax, Tunisia
**Laboratory of Material Science and Environment (LMSE)-Faculty of Science of Sfax (University of Sfax) 3038 Sfax-Tunisia

(*Received 27 April 2021 • Revised 19 July 2021 • Accepted 15 August 2021*)

Abstract−This research work is based on the isolation of cellulosic fibers from Tunisian olive sawdust (TOS) by alkaline treatment using a solution of NaOH at different concentrations: 5% w/v (TOS5) and 20% w/v (TOS20). The valorization of these cellulosic supports was assessed by the adsorption ability of methylene blue (MB), chosen as a model compound of organic dyes. SEM and FTIR analyses have shown that alkaline treatment produces a delignification of TOS and an elimination of hemicellulose. A transformation of cellulose I to cellulose II was shown by XRD following the decrease of the crystallinity indices passing from TOS5 (~37%) to TOS20 (~30%). The spectroscopic study confirmed that the intermolecular and intramolecular hydrogen bonds have a primordial role in the forms and the structural stability of the cellulosic substrates. Thereby, the deconvolution of OH stretching vibration band confirmed the transition from cellulose I to cellulose II by the occurrence of a new band at 3,080 cm^{-1} for TOS20. The increase of iodine adsorption values (ISV) from 40 $mg \cdot g^{-1}$ for TOS5 to 65 $mg \cdot g^{-1}$ for TOS20 is behind the improvement of the accessibility of cellulosic support with alkaline treatment of TOS. The adsorption of MB onto the surface of cellulosic substrates in aqueous mixtures was studied quantitatively. The corresponding isotherms in basic medium have shown the formation of a monolayer following the Langmuir model characterized by 14 $mg \cdot g^{-1}$, 52 $mg \cdot g^{-1}$ and 76 $mg \cdot g^{-1}$ onto the TOS, TOS5 and TOS20, respectively. The desorption efficiency of MB in acid medium increased with 37%, 57% and 71% for TOS, TOS5 and TOS20, respectively. Hence, the extracted cellulosic fibers are likely to be a promising adsorbent for the removal of organic dye from aqueous solutions.

Keywords: Olive Sawdust, Alkaline Treatment, Cellulose, Crystalline Structure, Organic Dyes, Absorption

INTRODUCTION

The rejection of wastewater has been considered as a serious problem because of its environmental impact [1]. Its properties such as color, high content of organic compounds, high carbon oxygen demand (COD) and the presence of suspended solids have caused harmful problems that have increased in recent decades [2,3]. The latter has several diversified sectors, especially the textile industry, which represents one of the most important economic sectors in Tunisia [4]. However, the high water consumption associated with this sector (up to 150 liters of water per 1 kg of dyeing cotton) and the production of wastewater [5] has hampered the success of this sector. The wastewater discharged by this industry is characterized by a complex composition (dyes, toxic heavy metals, and inorganic materials) [6]. When it is ejected, certain textile effluents contaminate surface and groundwater and endanger human health. In spite of this fact, such industrial wastewaters must be imperatively ejected. During the past thirty years, research studies have been increasingly carried out to limit this source of pollution using common processes, such as biological treatment [7]. However, microorganisms are unsuitable in the case of synthetic dyes, which are bio-refractory. Many techniques have been applied, namely membrane filtration [8], extraction with solvent [9,10], chemical methods such as Fenton oxidation [11], ozonation [12], photocatalytic degradation [13] and nano-photocatalytic technologies using self-assembled nanostructures [14-16]. Among the alternative physicochemical processes, adsorption remains a relatively used method that is easy to implement [17-19,20-26].

Activated carbon is the most manufactured adsorbent and the most industrially used for organic and inorganic pollutants [17-19]. Its usefulness emanates mainly from its well-developed internal microporosity of a large surface area ranges from 500 to 1,500 $m^2 \cdot g^{-1}$ [27]. Over the past years, many researchers have focused on the preparation of bio-adsorbents from agricultural by-products (lignocellulosics), especially natural waste to replace activated carbon. These bio-adsorbents available with a virtually zero cost have proven to be effective against many organic molecules, such as Kenaf [20] date kernels and palm fiber [21], treated olive pulp [22], sawdust and wood chips [23]. In our previous study, we demonstrated the feasibility of sawdust use as a low-cost adsorbent. Furthermore, it has been shown that this adsorbent can be easily electrochemically regenerated. Besides, multiple adsorption and regeneration cycles lead to the activation of sawdust by polarization [24].

†To whom correspondence should be addressed.
E-mail: makki.abdmouleh@fss.rnu.tn

Sawdust is one of many bio-adsorbents used in the adsorption of organic matters [25] and metals [26]. It is generally recovered by the rejection of joinery in the furniture and buildings industry. Sawdust contains mainly hydroxyl groups and carboxylic acid functions [28]. This chemical heterogeneity confers it an acid-base character that determines its electric charge [29]. Sawdust is a biomaterial with a complex chemical composition and a high surface heterogeneity that is mainly composed of cellulose, hemicellulose, lignin and extractable substances with a minor fraction [28]. The proportion of these constituents differs from one fiber to another. Its chemical composition depends not only on the nature of fibers but also on the growth condition, the age of the plant, climatic conditions [30]. The chemical composition taken from the literature for wood is cellulose (40-47%), hemicellulose (25-35%), lignin (16-31%) and extractable substances (2-8%) [30,31]. Cellulose extraction leads to the removal of lignin and hemicellulose from agricultural raw materials waste [32]. Cellulose is the most abundant naturally occurring and the most technologically interesting polymer. Besides, it is one of the promising raw materials available, in terms of cost for the preparation of various functional materials [33,34].

The property which determines the importance of the use of cellulose and its derivatives as a bio-adsorbent is the presence of hydroxyl functions groups considered as the most reactive of the cellulosic units. Actually, one of these hydroxyls is primary and the two other hydroxyls are secondary. These three groups involved in inter- and intra-molecular hydrogen bonds with neighboring chains can be modified by physical and/or chemical transformation for various applications [35]. Several chemical treatments modifying the surface functions of cellulose have been the subject of many research works [36,37]. The most used treatment is the alkaline treatment. According to ASTM D1965, this process consists of interacting fibers with a concentrated solution of a strong base to have a significant swelling resulting from changes in fine structure, size, morphology and mechanical properties [38,39]. The type of alkaline solution (KOH, LiOH, NaOH) and its concentration are the among parameters which would act on the effectiveness of the alkaline treatment as well as on the degree of swelling and that of the lattice transformation into cellulose-II [32]. Studies have shown that Na^+ has a favorable diameter able not only to enlarge the smallest pores between the planes of the lattice but also to penetrate them. Therefore, the treatment with sodium hydroxide (NaOH) leads to an increased swelling [38]. Referring to the literature, the treatment with a characteristic concentration of aqueous NaOH solution (≈10 wt%) leads to a polymorphic transformation of cellulose I to Cellulose II (mercerization) [40,41]. The mercerization process is described as follows: In the first step, the water molecules penetrate into the amorphous regions of cellulose where the hydrogen bonds are broken. Then, the sodium hydroxide reaches the crystalline zones and reacts with the hydroxyl groups of the anhydroglucose unit of cellulose inducing the swelling of cellulose chains. Chains initially aligned in parallel for native cellulose I are rearranged into anti-parallel chains characteristic of cellulose II by twisting fibers [42]. The transformation of cellulose I into cellulose II goes through an intermediary called Na-cellulose I [43]. This intermediate structure has relatively large distances between the cellulose molecules and developed in cellulose amorphous region. In this structure, the -OH groups of the cellulose are converted into -ONa groups, enlarging the dimensions of the molecules.

The involved chemical reaction can be given by Eq. (1) [44]:

$$\text{Cellulose-OH}+\text{NaOH}\rightarrow(\text{Cellulose-O}^-)\,\text{Na}^+ + \text{H}_2\text{O impurities} \quad (1)$$

After this first step, Na-cellulose I becomes able to absorb more alkaline solution and then it is converted into Na-cellulose II with a helical structure. By washing the Na-cellulose II subsequently with water, all the Na-ion bonds are broken and the final structure of Na-cellulose IV is obtained which would be converted into cellulose II by drying [45]. The cellulose fibers of various microcrystalline forms extracted from different natural sources have been used as adsorbents of organic dyes or metal solutions [46,47]. Siroky et al. [46], studied the adsorption of reactive dyes on Lyocell fibers to understand the effect of alkali treatment on sorption behavior of cellulose II fibers. However, the adsorption of Cu^{2+}, Cd^{2+} and Pb^{2+} into modified non-mercerized and mercerized cellulose was done with succinic anhydride from aqueous single metal ion solutions [47].

The present research work contributes to the isolation of Cellulose-I and II from Tunisian olive sawdust by alkali treatment and the ability of native and treated sawdust to the adsorption of methylene blue. The sawdust under investigation is waste from olive wood obtained from Tunisia, which is located in the south of the Mediterranean, and known to be one of the most famous countries in the field of olive growing and olive oil exportation.

EXPERIMENTAL

1. Materials

Tunisian olive sawdust (TOS): The sawdust of olive wood "Chemlali" used in this study as an adsorbent was obtained from a furniture factory in the region of Sfax (Tunisia). It was in the form of corrugated chips of varying lengths. The crude sawdust was washed with distilled water several times to ensure that all suspended particles were removed from the wash water and then filtered. The washed TOS was dried in an oven at 100 °C and subsequently sieved to have a particle size in the range of 0.5 and 1 mm.

Methylene Blue (MB), a cationic dye, was used as the model compound for its high color intensity at low concentration. MB was purchased from Merck and used as received without further purification. The MB solutions at the desired concentration were prepared with ultra-pure water.

2. Isolation of Cellulose from TOS

The alkali treatment of TOS is presented in organogram (Fig. 1). A quantity of 20 g of sawdust (TOS) was treated with 1 L of NaOH solution for 6 h at 80 °C (in Universal Oven Memmert UN30). The concentrations of the NaOH solutions chosen were 5 and 20 wt%. The fibers bundles were then washed with alternating treatments of acetone and distilled water at ambient temperature (≈24 °C). The washing step was repeated several times by adding fresh quantities of water and acetone (50/50) until a neutral solution (pH=7) was obtained. The used pH meter was Consort l C931. A subsequent bleaching treatment was conducted to remove the residual lignin with a solution of NaClO. A solution of NaClO (1 : 1 V/V) (250 mL) was added to residual TOS (20 g) at

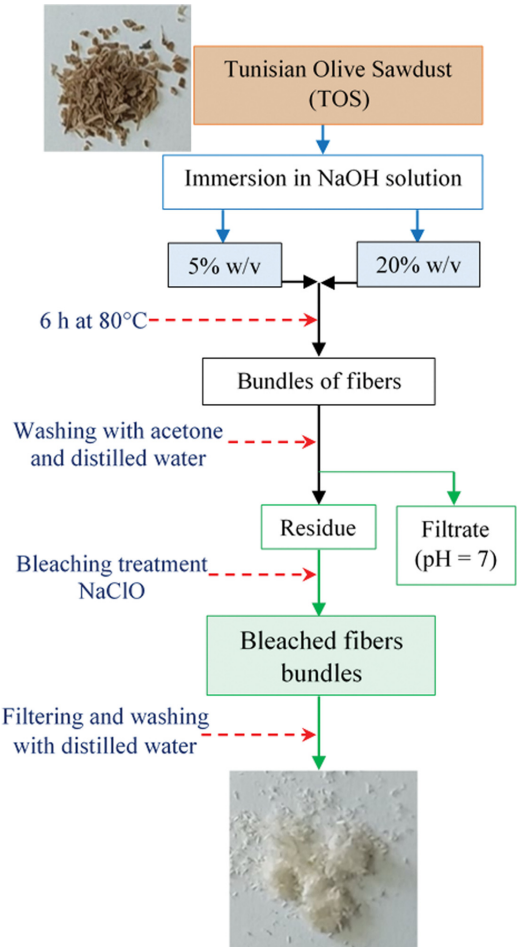

Fig. 1. Process schema of alkali treatment of Tunisian olive sawdust (TOS).

room temperature for 1 hour. The bleached fibers were filtered on paper filter and extensively washed with distilled water. Finally, the obtained fibers were dried at room temperature followed by drying in a vacuum oven for 48 h at 80 °C.

INSTRUMENTATION AND CHARACTERIZATION

1. Morphological Characterization (SEM)

The morphology of TOS before and after alkali treatment was characterized by a scanning electron microscope (SEM) using a ZEISS-ULTRA55 SEM microscope. The sample was coated with gold layer and observed using an applied tension of 1 kV.

2. FTIR Spectroscopy (ATR)

To identify the functional groups, untreated and treated TOS were analyzed using a Perkin Elmer FTIR system spectrum BX using an ATR mode within the range of 4,000-500 cm^{-1}.

3. X-ray Diffraction (XRD)

The structure and crystallographic properties of native sawdust (TOS) and mercerized fibers (TOS5 and TOS20) were characterized by X-ray diffraction using a SIEMENS D5000 automated wide-angle powder X-ray diffractometer and CuKα radiation (λ= 1.5406 Å). The intensity diffracted by the sample was collected by a detector covering a range from 2° to 12° and the X-ray spectra were recorded between 5 and 35°.

4. Thermogravimetric Analysis (TGA)

Thermogravimetric analysis (TGA) of the raw and treated TOS was realized on a Perkin-Elmer TGA7 analyzer. The heating rate was 10 °C/min and the sample weight was in the order of 4 mg. Thermograms were recorded over a temperature range of 30-530 °C carried out under an oxygen atmosphere with the flow rate of 20 ml/min.

5. Accessibility (Determination of the ISV)

Empirically, the fiber accessibility by reagents is determined by the iodine sorption value (ISV) test. According to Nelson [48,49], 50 mL of iodine solution (0.1 $mol{\cdot}L^{-1}$) and 50 mL of saturated sodium sulfate solution were added accurately to a given weight w (g) of the raw and treated TOS samples. The system was stirred using mechanical shaker for 1 h at 23 °C±1 °C and filtered. Then, 50 mL of the filtrates was titrated using Sodium hyposulfite standard solution (0.01 $mol{\cdot}L^{-1}$) in the presence of 1% starch as the indicator. The blank experiment was carried out with the same operation. The ISV in mg I_2/g cellulose was calculated according to Eq. (2).

$$ISV\ (mg_{iodine}/g_{cellulose}) = \frac{T_s - t_s}{w} \times N \times F \times 126.91 \quad (2)$$

where $T_s = T_b \times (I_s/I_b)$ is the amount of thiosulfate solution ($Na_2S_2O_3$) solution equivalent to the initial iodine in aliquot of sample solution (mL); I_s, the weight of concentrated iodine-potassium iodide (I_2-KI) solution in a sample solution (g); I_b, the weight of concentrated I_2-KI solution in a blank solution (g); T_b, the amount of $Na_2S_2O_3$ solution for aliquot of blank solution (mL). t_s is the amount of $Na_2S_2O_3$ solution for aliquot of supernatant filtered from sample (mL); F, the aliquot factor considering that the total volume of sample solution was 102 mL; N, the concentration of $Na_2S_2O_3$ (mol/L); W, the oven-dry weight of sample (g).

6. Methylene Blue Adsorption Application

The adsorption study of Methylene Blue (MB) onto raw and treated TOS was carried in a batch reactor using a thermostatically controlled cell. The determination of MB concentration was carried out by UV-visible spectrophotometer at a wavelength of 663 nm using a UNICAM UV4 UV/Vis spectrophotometer. The adsorption isotherms were obtained at room temperature with different initial concentrations of MB using TOS, TOS5 and TOS20.

7. Desorption Study

For desorption studies, TOS cellulosic substrates were mixed with 400 $mg{\cdot}L^{-1}$ of MB solution (pH=10) at room temperature (298 K). The residual MB concentration in the solution was measured to calculate dye adsorbed on the adsorbent. Then, MB loaded adsorbent was dried and added to 10 mL of distilled water at various pH values (pH 2, 7 and 10) in 50 mL conical flaks. These flasks were agitated on the orbital shaker at 150 rpm for 15 min. The MB dye desorption capacity (qe, desorption, $mg{\cdot}g^{-1}$) was determined by the same method of assaying adsorbed MB. As for the desorption efficiency D of MB dye, it was calculated using Eq. (3):

$$D(\%) = \frac{q_{deso}}{q_{ads}} \times 100 \quad (3)$$

where q_{ads} and q_{deso} are the quantities of adsorbed and desorbed of

MB, respectively.

RESULTS AND DISCUSSION

1. Morphological Analysis

Changes in the fine structure of raw and treated TOS samples were observed from scanning electron micrographs (SEM) as shown in Fig. 2. Sawdust (TOS) is a lignocellulosic composite fiber (Fig. 2(a)), which consists of crystalline cellulose and amorphous cementing materials: hemicellulose and lignin. The morphology for untreated sample (TOS) is homogeneous with better bonding between cellulose and the matrix. In fact, the surrounding fibers were linked together and their bundles were composed of adhered pectic and hemicellulosic tissues and incorporated lignin. The fiber lumen is not so well defined. However, after alkali treatments with different concentrations of NaOH (Fig. 2(b) and Fig. 2(c)), the fibrous structure is well observed on SEM images of TOS5 and TOS20. Thus, the fibers are becoming increasingly convoluted and the lumens are well defined with the increase in alkali treatment. The matrix is abducted due to removal of noncellulosic compound. The morphology of fiber in TOS5 and TOS20 sample indicates a conversion of the surface into a swollen and straightened state, indicating that the assembly and orientation of microfibrils were completely changed. The roughened surface of treated fibers was a direct result of removed hemicellulose, lignin and wax from the alkali treatment [44,50].

2. XRD Analysis

To evaluate the structural changes in the cellulose before and after the alkaline treatment, X-ray diffraction (XRD) measurements were carried out for raw and treated TOS (Fig. 3). Following the decon-

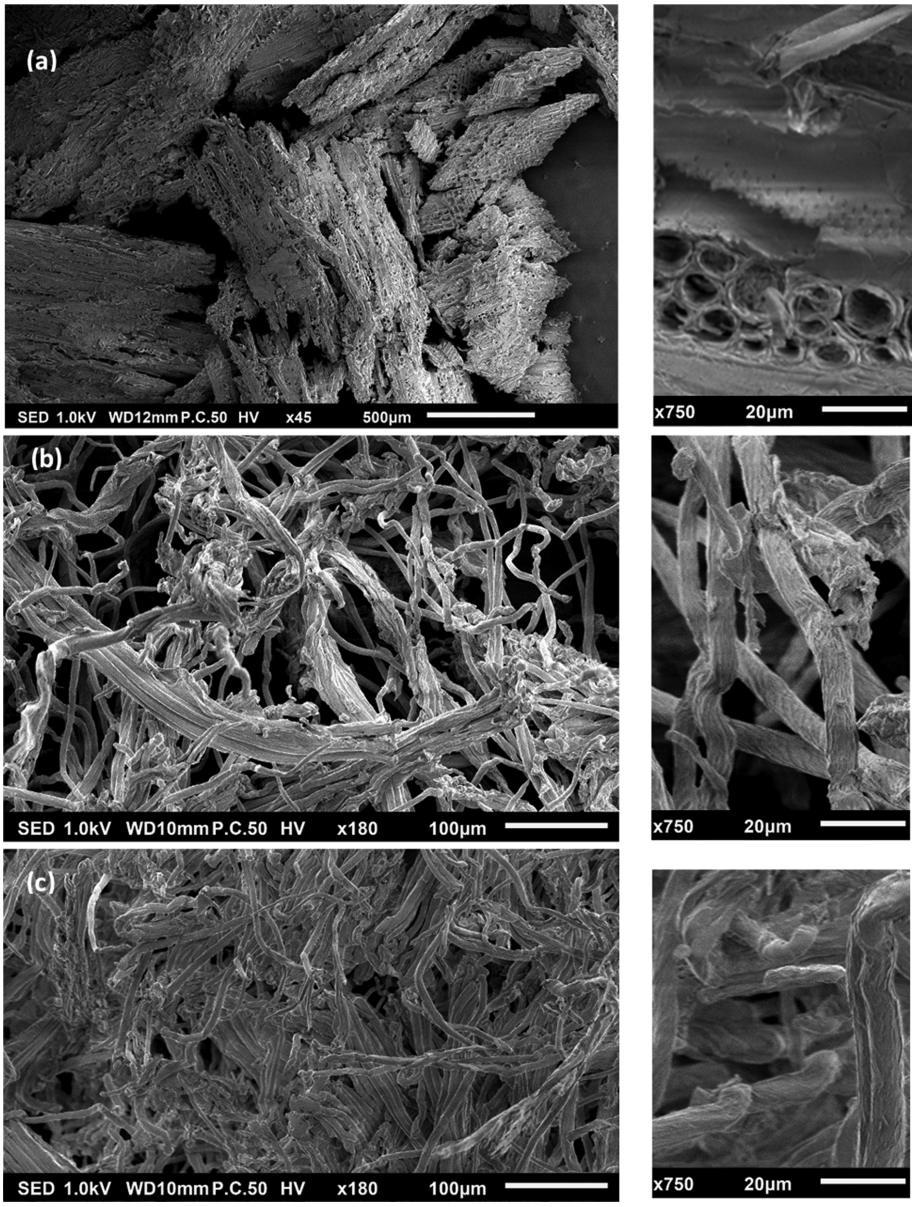

Fig. 2. SEM images at different magnification of: (a) Sawdust (TOS), (b) Cellulose I (TOS5) and (c) Cellulose II (TOS20).

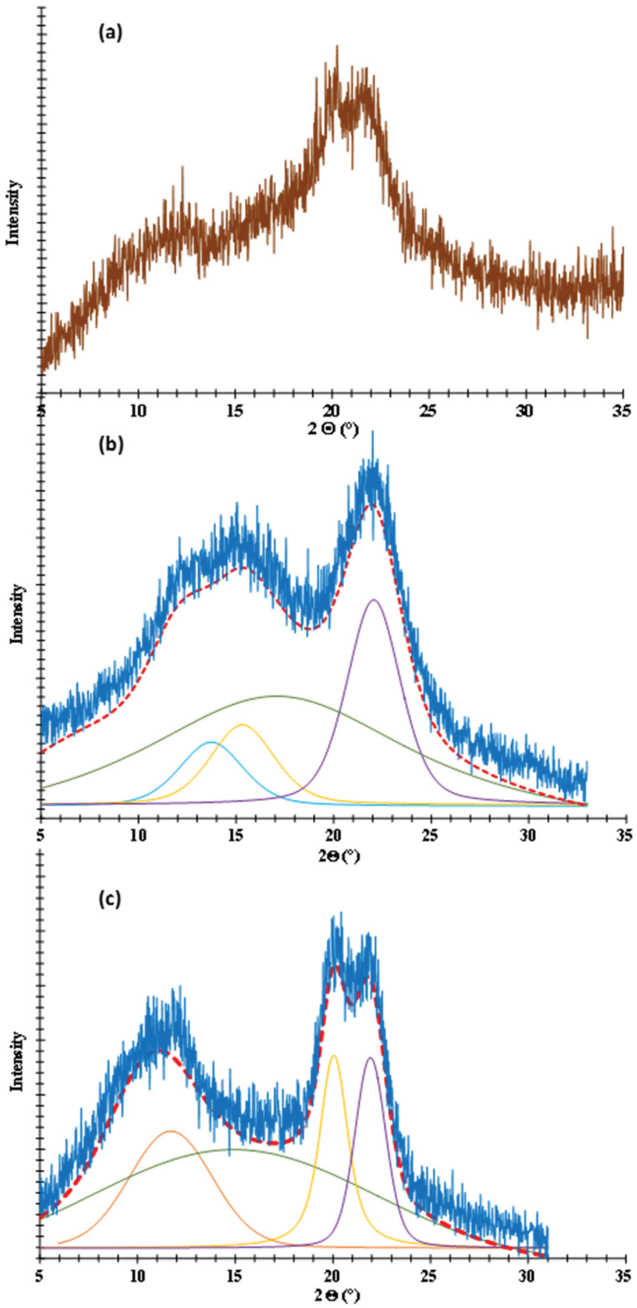

Fig. 3. XRD pattern of (a) sawdust (TOS), (b) Cellulose I (TOS5) and (c) Cellulose II (TOS20).

volution of the diffractograms, the individual peaks were adjusted by the Gaussian functions.

A review of the X-ray diffraction pattern in Fig. 3(b) indicates the typical appearance of cellulose I. The deconvolution of the X-ray diffractograms shows the presence of three peaks located at 2θ=14.36°, 15.46° and 21.98°, which corresponds to crystallographic reflection planes (101), (10$\bar{1}$) and (002), respectively [35,50]. The amorphous region is represented by a very broad peak centered at about 18°. The increase of the concentration of sodium hydroxide during the treatment of TOS generated a significant variation on the TOS20 diffractogram (Fig. 3(c)). The peak of the crystallographic reflection plane (002) was divided into two weaker peaks located at 20.2° and 21.7°. The deconvolution of the DRX showed that it was composed of four peaks located in 2θ at 12.16°, 20.2°, 21.7° and 35.06° corresponding to (101), (10$\bar{1}$), (002) and (040) crystallographic planes, respectively, indicating the formation of cellulose II [51] and a fifth very large peak relating to the amorphous region around 19°.

Table 1. TOS crystallinity index before and after the alkaline treatment by applying two methods: A and B

Samples	CI (%)	
	Method A [51]	Method B [52]
TOS	30.51	---
TOS5 (CI)	39.45	36
TOS20 (CII)	30.16	30

In the literature, several methods have been based on the use of the diffractogram to calculate the crystallinity index (CI) of cellulosic fibers [49]. First, we adopted the Segal method, designated as method A, according to which the crystallinity index CI_A (%) was determined using the empirical Segal Eq. (4) [51].

$$CI_A(\%) = \frac{I_{002} - I_{am}}{I_{002}} \times 100 \quad (4)$$

I_{002} is the maximum intensity of the crystallographic reflection plane (002) (2θ between 22° and 23°) and I_{am} is the maximum intensity of the X-ray scattering band due to the amorphous part of the cellulose located between 18° and 19° where the intensity is minimum.

The second method to find the crystallinity index (named method B) is based on DRX curve fitting [52]. The sum of the area under the adjusted crystalline peaks (I_c) and the broad amorphous peaks (I_{am}) was used to calculate the crystallinity index CI_B (%) according to Eq. (5).

$$CI_B(\%) = \frac{I_c}{I_c + I_{am}} \times 100 \quad (5)$$

The crystallinity index CI_A values for raw TOS, treated with TOS5 and TOS20 were 30.51% 39.45% and 30.19%, respectively (Table 1). An increase in the CI_A for the treatment of TOS with 5% NaOH was observed. In fact, for a low concentration of NaOH, the alkaline treatment led to the removal of amorphous areas of the wood by removing hemicellulose and lignin in large part [44,53]. However, the decrease of CI_A at the high concentration of soda (20% w/v) is related to the change in the microstructure of cellulosic fibers. Indeed, the phenomenon of mercerization had occurred by modifying the fine structure and morphology of the fibers as well as the conformation of the cellulose chains. During this process, soda entered in the cellulose fibers and participated in the swelling of the fibrous structure of the material. The polysaccharide chains are rearranged from native cellulose I (chains aligned in parallel) to cellulose II (antiparallel), leading to the increase of the less ordered areas with the decrease of the crystalline area [42,54].

3. FTIR Analysis

The FTIR spectra of untreated and treated TOS, TOS5 and

TOS20 are illustrated in Fig. S1 After the alkaline treatment of TOS, the bands corresponding to the groups C=O (1,730 cm^{-1}), C-H (1,236 cm^{-1}) and C=C (1,504 cm^{-1}) disappeared on the TOS5 and TOS20 spectra, confirming the removal of hemicelluloses and lignin by hydrolysis in an alkaline solution [35,54]. Likewise, the delignification of TOS was confirmed by the decrease in the intensity of the bands situated at a wavenumber around 830 cm^{-1} and 1,431 cm^{-1} characterizing the out-of-plane C-H aromatic vibration [55] and the CH_2 symmetric bending of lignin, respectively. On the other hand, the absence of lignin compared to cellulose for the TOS5 and TOS20 was justified by the increase of the band intensity situated at 897 cm^{-1} characteristic of the symmetrical elongation of the β-glucosidic linkage C-O-C.

The band situated at 1,645 cm^{-1}, observed on the three spectra, is attributed to the deformation vibration of water OH groups. The increase of intensity and the widening of this band as a func-

Table 2. 1,550-1,180 cm^{-1} spectra region linked to the transformation cellulose I (cell I) into cellulose II (cell II) by the alkaline treatment of TOS and vibration assignment of each band

TOS5	TOS20
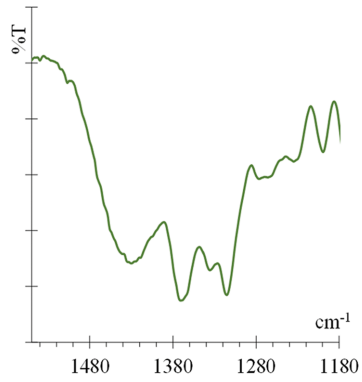	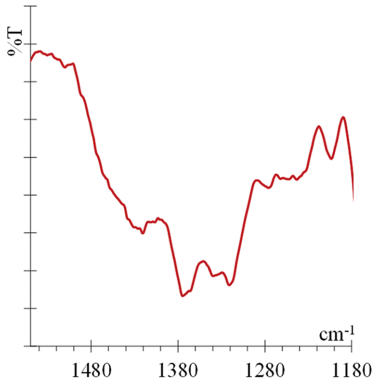

Vibration assignment	Frequency (cm^{-1})		References
	Cell I	Cell II	
-OH in plan bending	1205	1200	[35,60]
CH bending	1282	1278	[60,61]
CH_2 wagging	1317	1315	[35,61]
-OH in plan bending	1336	1335	
CH bending	1375	1375	[35,61]
CH_2 symmetric bending	1420	1420	[61,62]
-OH in plan bending	1455	1470	

Table 3. 3,050-2,700 cm^{-1} spectra region linked to the transformation cellulose I into cellulose II by alkaline treatment of TOS and vibration assignment of each band

TOS5	TOS20
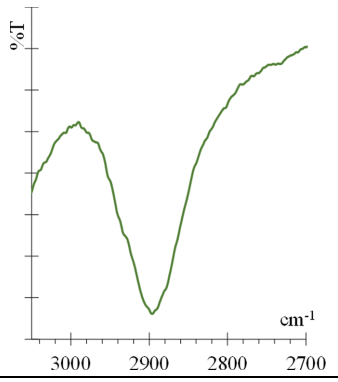	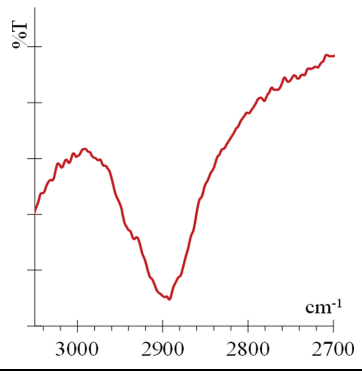

Vibration assignment	Frequency (cm^{-1})		References
	Cell I	Cell II	
CH stretching	2,892	2,896	[59,64,65]

Table 4. 3,750-2,950 cm^{-1} spectra region linked to the transformation cellulose I into cellulose II by alkaline treatment of TOS and vibration assignment of each band

TOS5	TOS20
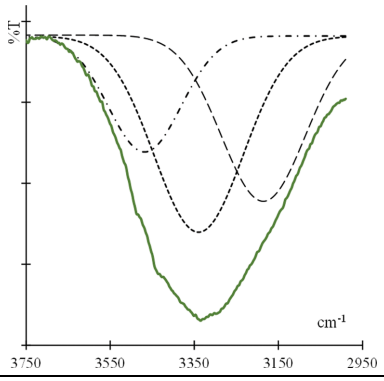	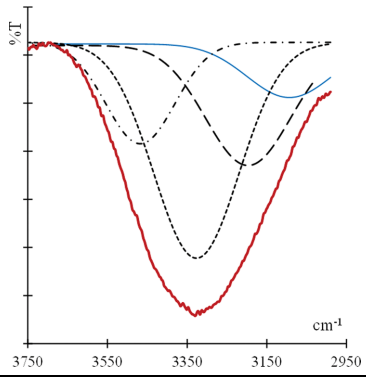

Vibration assignment	Frequency (cm^{-1})		References
	Cell I	Cell II	
-OH stretching (hydrogen bond)	3,460 3,328 3,175	3,453 3,316 3,175 3,080	[57-59,64]

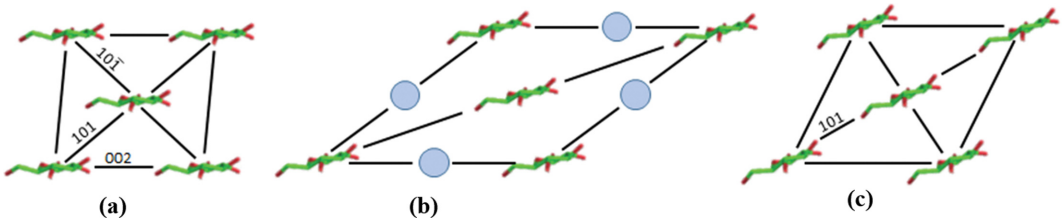

Fig. 4. The transformation of cellulose I (a) to cellulose II (c) takes place via Na-cellulose I (Na is grey circle) (b): Cross-section view of the elementary lattice cell and index designation according to Meyer and Misch (assuming a parallel chain arrangement for all lattices) [33,66,71].

tion of the degree of alkaline treatment is probably related to the increase in the hydroxyl groups accessibility of the cellulosic structure against water molecules [56].

The region situated between 1,200 cm^{-1} and 1,550 cm^{-1} (Table 2) containing several bands seemed to be affected not only by the amorphous content of fibers but also by the type of crystal lattice [57]. The peaks which had a move from TOS5 to TOS20 were those of approximately 1,372, 1,335 and 1,315 cm^{-1} [58]. The little move of these peaks towards a low wavenumber confirms the dominance of cellulose I and cellulose II over the fibers of TOS5 and TOS20, respectively. Similarly, the decrease in the intensity of the CH_2 bending band reflects a higher number of disordered crystals in the TOS20 pertaining to the formation of cellulose II [35,59].

The range of wavenumbers from 2,500 to 3,700 cm^{-1} is strongly influenced by the alkaline treatment (Table 3). Among the bands whose absorbance had strongly changed during the alkaline treatment were those attributed to the intermolecular and intramolecular hydrogen bonds. Thus, the intensity (% T) of the CH stretching band moved from 2,896 cm^{-1} for TOS5 to a wavenumber less than 2,892 cm^{-1} for TOS20 (Table 2). The decrease in wavenumbers at this position was probably due to small changes in the angles of twist, affected by the hydrogen bonds, β-1,4-D-glycosidic bonds [63]. Indeed, the intermolecular and intramolecular hydrogen bonds have a primordial role in the structural stability of the cellulosic supports affecting the vibration movements of the hydroxyl groups in IR. Thus, the theoretical resolution of hydrogen-bonded OH stretching following the Gaussian distribution of the spectral region of 3,000-3,700 cm^{-1} (Table 4) reveals that the mixed modes of O-H elongation are resolved in three bands for TOS5 and four bands for TOS20. In fact, compared to the TOS5 bands, the new band (in blue on Table 4) which appears on the TOS20 spectrum around 3,080 cm^{-1} is attributed to the vibration of the -OH groups in intermolecular hydrogen bond characteristic of cellulose II [35]. The transition from cellulose I to cellulose II for TOS5 and TOS20, respectively, is also confirmed by the little moves of the bands around 3,215, 3,328 and 3,460 cm^{-1} [35,63].

The significant changes in the IR spectra related to the transformation of cellulose I (TOS5) to cellulose II (TOS20) take place via Na-cellulose I (Fig. 4), which is responsible for the swelling of cellulose inducing the expansion of its lattice [66,67]. We report that cellulose I simultaneously contains the I_α form whose triclinic crystal lattice has one chain, and the I_β form with monoclinic crystal

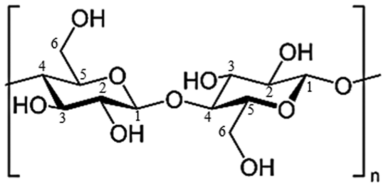

Fig. 5. Molecular structure of a cellulose unit, showing the β 1-4 glucosidic bond with the indexation of carbon atoms.

lattice has two chains. The two forms I_α and I_β are arranged in a parallel fashion forming the crystal structure of cellulose I [33,68]. When cellulose is mercerized or dissolved and then precipitated, a different crystal structure, called cellulose II, appears. It exhibits an antiparallel arrangement in the two-chain monoclinic crystal lattice [33]. In fact, the transformation from cellulose I into cellulose II in the TOS5 and TOS20 structures, respectively, is at the origin of the rupture not only of the intermolecular hydrogen bonds (plane 002) but also of the intramolecular ones. Then, the inclusion of NaOH and water in the cellulose chain lattice, combined with a rotation of the molecular chains, leads to an increase in the distance between cellulose molecules. According to the rotation of the chains, new intermolecular hydrogen bonds are formed on the plane (101) during the elimination of the soda (during washing) and the formation of the cellulose II lattice. The rupture of the intramolecular hydrogen bonds O(2)H---O(6) and O(3)H---O(5) implies a detachment of the fixation of glycosidic bond C (l)-O-C(4) (Fig. 5). This means that the conformational change of the molecular chains during the transformation of cellulose I into cellulose II as found in various studies [69,70] is obtained by breaking the intramolecular hydrogen bonds. The formation of new inter- and intramolecular hydrogen bonds is indicated by a change in the absorbance bands which reach a different domain from that of cellulose I.

4. Thermogravimetric Analysis

To compare the influence of alkali treatment on the stability of cellulose fibers extracted from TOS, thermogravimetric analyses were conducted (Fig. S2). Contrary to TOS5 and TOS20, the presence of inflection point at 310 °C on the TOS thermogram can be attributed to the decomposition of hemicellulose present in raw olive sawdust. Also, compared to TOS5 and TOS20, TOS degrades over a wide temperature range from 200 °C to 500 °C with a residual mass of 9% for temperatures above 500 °C. This is mainly linked to the heterogeneity of the native wood composition, by the presence of lignin and mineral components [72]. For the three cellulosic supports TOS, TOS5 and TOS20, a small loss of mass was observed over the temperature range of 30 °C and 200 °C due to the vaporization of the adsorbed moisture water. After alkaline treatment, these losses of moisture had a greater value for TOS20 (8%) compared to TOS5 (4%). This is due to the effect of the variation in crystallinity that decreased in favor of the amorphous zone for TOS20 that is probably more accessible to water molecules from the atmosphere.

5. Accessibility

The study of iodine adsorption used in the present work is a classical method for the determination of the accessibility degrees, which takes place in less ordered amorphous regions of cellulose [48-49]. The iodine adsorption values (ISV) for the cellulosic supports TOS5 and TOS20 at room temperature are 40 and 65 mg/g, respectively. The increase in ISV for TOS20 compared to TOS5 fibers is related to the fact that (i) swelling of the fiber structure by alkaline treatment can help increase the fibers accessibility, and (ii) alkaline pretreatment can disrupt the primary walls of the fibers and damage the intra and intermolecular hydrogen bonds, thereby liberating hydroxyl groups and transforming the fractionated crystallization zone into an amorphous zone [73]. Through these results, the predominance of the Cellulose I and Cellulose II structure in the TOS5 and TOS20 samples, respectively, has been confirmed once again.

6. Methylene Blue Adsorption

Although cellulose fiber is a porous polymer with a wide pore size distribution, the hierarchical and aggregated winding structures cause poor accessibility and reactivity of cellulose substrates with chemical reagents. By the swelling of fibers in a basic medium, the hydroxyl bonding strength would be weakened, which would improve the rate of reagent diffusion inside the cellulose fibers. The initial pH of MB solution is an important factor in the adsorption process. Therefore, different pH medium was used to evaluate the relative pH at high adsorption of MB. The initial pH of the solutions was adjusted ranging from 2 to 13 by adding the aqueous solutions of sulfuric acid and/or sodium hydroxide (1 M). The amounts of dye adsorbed by TOS were evaluated by calculating the percentage of MB removed R(%) expressed in Eq. (6):

$$R(\%) = \frac{C_0 - C_f}{C_0} \times 100 \quad (6)$$

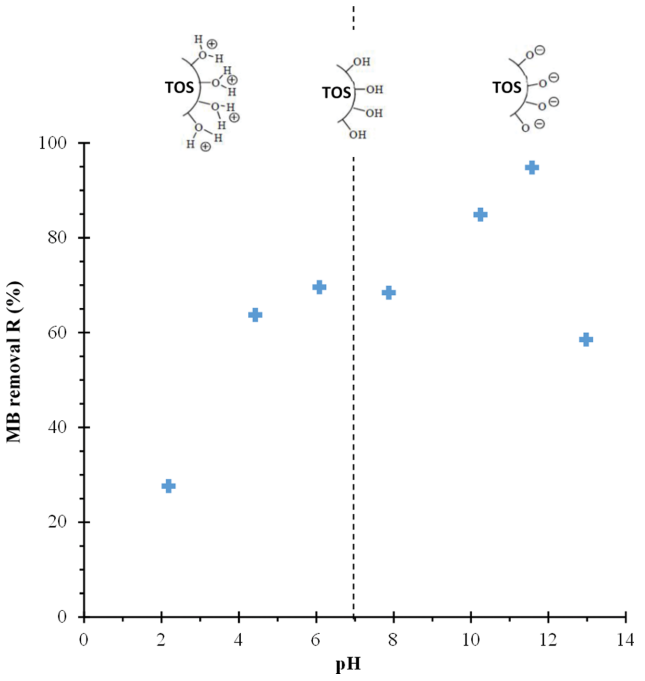

Fig. 6. Effect of pH on the MB removal by TOS; m_{TOS}=250 mg; C_0= 300 mg·L^{-1}; V_{sln}=20 mL; T=20 °C; w=450 rpm. Relative schema of the charge carried by the TOS surface as a function of the pH.

where C_0 and C_f denote the absorbance of the solution before and after treatment, respectively.

6-1. Effect of pH

The examination of Fig. 6 shows that the removal percentage increases initially and tends to stabilize around the pH=6. Then, it increases again from pH=9 to reach the maximum value of 95% approximately at the pH 11.5. Beyond this value, the percent of MB removal decreases reaching 55% at pH=13. According to the literature, these results could be explained by the fact that the TOS contains polar groups such as hydroxyl and carboxyl. Thus, the electrical charge of the adsorbent surface depends on the pH of the reaction medium, following the ionization of these surface functional groups [74]. Therefore, in a very acidic medium, the surface charge of wood support as TOS might be positive. Consequently, its interaction with MB solution, which is also positively charged (pka=3.8) is weak. By increasing the pH of the solution over the pH range 9 to 11.5, the charge of the adsorbent becomes more negative. This enhances the attraction between MB and TOS surface. However, the decrease of dye adsorption at higher pH value might be explained by the delignification of the TOS at strongly basic pH, hence the progressive disappearance of the adsorption sites [74]. To optimize the removal of MB, the pH medium of solution for the raw and treated TOS was adjusted to 10.

6-2. Effect of Contact Time

To evaluate the maximum absorption time of MB at basic pH by TOS adsorbent, an adsorption kinetic study was accomplished. The variation of the MB removal percent R (%) and the adsorbed quantity q_{ads} of MB as a function of time is shown in Fig. 7. The quantities of adsorbed MB (q_{ads} expressed in mg of adsorbed MB per g of TOS ($mg{\cdot}g^{-1}$)) are calculated using Eq. (7):

$$q_{ads} = \frac{(C_0 - C_f) \times V_{sln}}{m_{TOS}} \quad (7)$$

where C_0 and C_f represent the concentration of the adsorbate in solution before and after treatment ($mg{\cdot}L^{-1}$), respectively, V_{sln} the volume of the solution (L) and m_{TOS} the mass of the TOS (g). The change in the percentage of MB removal of the solution increased rapidly as a function of time to reach a palate of 95% after 45 min. The adsorbed quantity of MB onto TOS increased linearly at the beginning of the treatment then increased slowly to stabilize and reach equilibrium at 45 min. The amount of adsorbed MB onto TOS was 22 $mg{\cdot}g^{-1}$. To provide information on the adsorption mechanism, pseudo-first order [75] and pseudo-second order [76] models of adsorption kinetics were investigated. The pseudo-first-order kinetic model can be expressed by Eq. (8) [75]:

$$Ln(q_{e1} - q_t) = Ln(q_{e1}) - K_1 t \quad (8)$$

where q_t ($mg{\cdot}g^{-1}$) is the adsorbed amount of MB at time t, q_{e1} ($mg{\cdot}g^{-1}$) is the maximum adsorption capacity, and k_1 (min^{-1}) is the rate constant of adsorption. Pseudo-first-order constants have been determined by the extrapolation of the plot $ln(q_e - q_t)$ vs (time) (Fig. 8(a)).

The linear form of the pseudo-second-order kinetic equation could be expressed by Eq. (9) [77]:

$$\frac{t}{q_t} = \frac{1}{K_2 q_{e2}^2} + \frac{1}{q_{e2}} t \quad (9)$$

where q_{e2} ($mg{\cdot}g^{-1}$) is the maximum adsorption capacity, and k_2 ($g{\cdot}mg^{-1}{\cdot}min^{-1}$) is the rate constant adsorption. Pseudo-order constants were determined by the extrapolation of the plot (t/q_t) vs (time) (Fig. 8(b)).

The k_1, k_2, q_1, q_2 and correlation coefficients R_1^2 and R_2^2 of MB were calculated and summarized in Table 5.

Fig. 8 and Table 6 show that the correlation coefficients (R_2^2= 0,99) for the pseudo-second order kinetic model are bigger than the coefficients (R_1^2=0,95) for the pseudo-first-order kinetic model. On the other hand, by applying the pseudo-first order model, the calculation of q_e for the two substrates shows that the amounts of adsorbed dye are rather low compared to the experimental amounts. The obtained results revealed that the adsorption fits better with

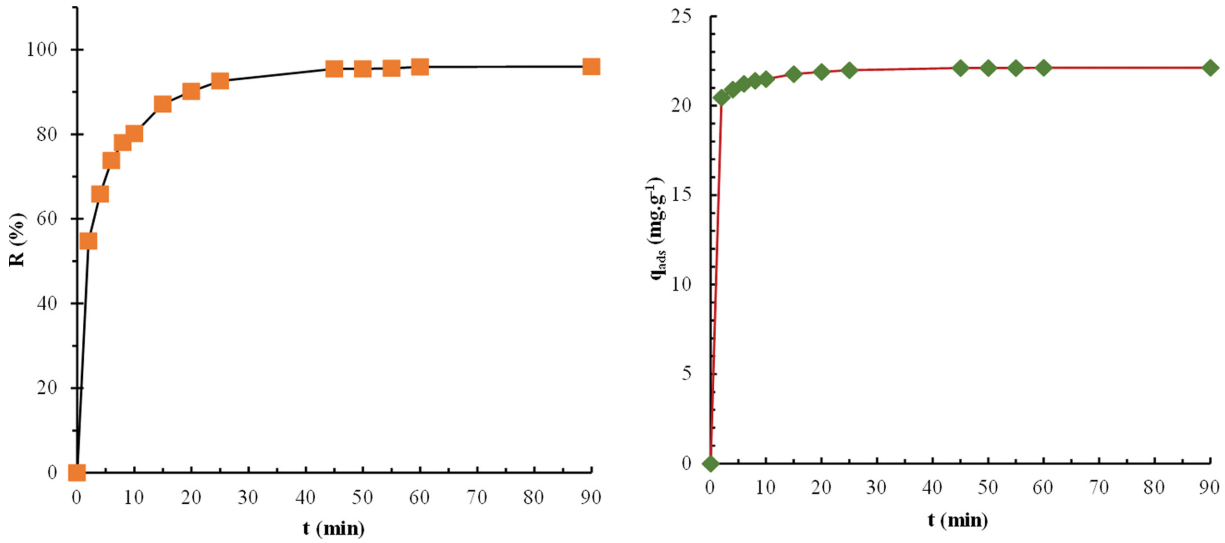

Fig. 7. Adsorption kinetics for methylene blue (MB) onto TOS: Variation of the MB removal percent (■) and the MB adsorbed quantity (◆). pH=10, m_{TOS}=1,5 g; C_0=300 $mg{\cdot}L^{-1}$; V_{sln}=100 mL; T=20 °C; v=450 rpm.

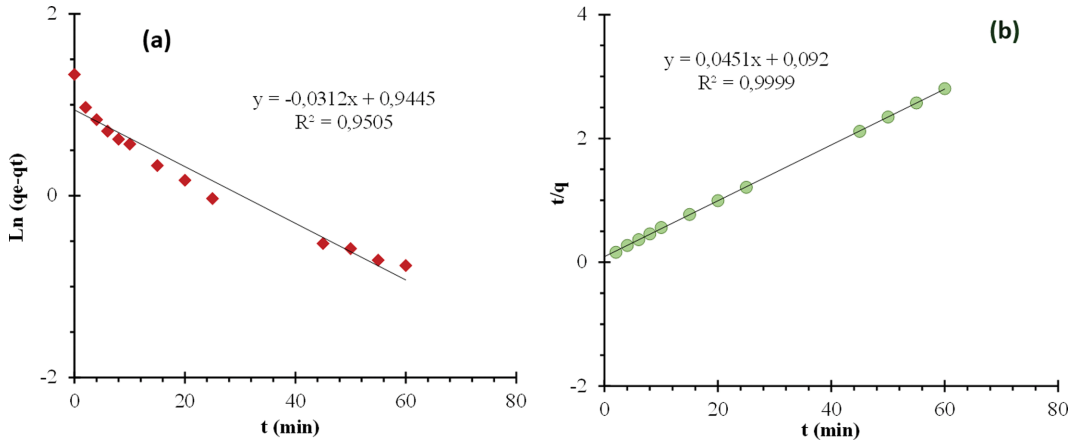

Fig. 8. Adsorption kinetic models for MB removal using TOS: (a) First-order plots, (b) second-order plots.

Table 5. Kinetic parameters of the pseudo-first order and the pseudo-second order models for MB adsorption into TOS

Pseudo-first order				Pseudo-second order		
$q_{e(exp)}$ (mg·g^{-1})	q_{e1} (mg·g^{-1})	K_1 (min^{-1})	R_1^2	q_{2e} (mg·g^{-1})	K_2 (g·mg^{-1}·min^{-1})	R_2^2
22,1	2,57	0,031	0,95	22,22	0,022	0,999

Table 6. Results Related to the Adsorption of MB on TOS, TOS5 and TOS20

Adsorbent	Adsorption isotherms	Langmuir model			
	q_m (mg·g^{-1})	q_m (mg·g^{-1})	K_{ads} (L·mol^{-1})	R^2	ΔG^o (KJ·mol^{-1})
TOS	14	14.45	94.67	0,9893	−11.07
TOS5	52	50.50	125.4	0,9973	−11.80
TOS20	76	72.46	139.47	0,9982	−12.02

the pseudo-second-order kinetic model [76].

According to this kinetic study, the adsorbed quantity of MB remained constant after 15 min, which implied the establishment of the adsorption-desorption dynamic equilibrium. Therefore, in all the experiments adsorption, the reaction medium (adsorbate+ solvent+MB) was kept under stirring for 1 h before measuring the adsorption capacity.

6-3. Adsorption Isotherm: Effect of Cellulosic Support

The adsorption isotherms of MB on the raw and treated TOS substrate at room temperature were studied (Fig. 9). Actually, the adsorption isotherm describes the interaction of dyes with adsorbent, which is a determinant factor for the performance of adsorption processes. It expresses the amount of adsorbate on the adsorbent q_e (in mg·g^{-1} of adsorbent) according to the concentration of adsorbate remaining in solution C_e (in mg·L^{-1}). The values of the maximum adsorbed quantities and the different thermodynamic parameters are summarized in Table 6. The adsorption isotherms indicated that the amount of adsorbed MB increased with the increase of initial concentration C_0 and reached a plateau situated at about 14, 52 and 76 mg of adsorbed MB per gram of TOS, TOS5 and TOS20, respectively. In the low C_0 range, the adsorption of MB adsorbent was closer to the theoretical line corresponding to 100% adsorption, which indicates a higher affinity of MB to the raw and treated TOS. After a C_0 value of about 200 mg·L^{-1},

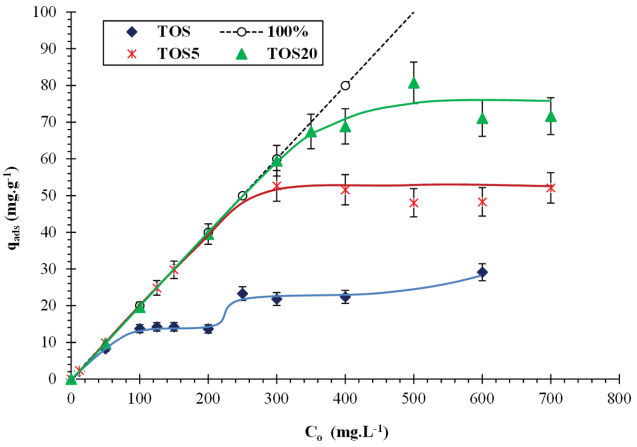

Fig. 9. The variation of the adsorbed amount at equilibrium as a function of the initial concentration of MB.

the adsorption started to increase and the isotherm form suggested the formation of multilayers for the TOS substrate. On the other hand, only one adsorption plateau was observed for both TOS5 and TOS20 after a C_0 value of about 350 mg·L^{-1}. The difference in MB behavior adsorption between raw and alkaline treated substrates is essentially due to the purity and the accessibility of

the materials. This phenomenon has also been considered during the alkaline dissolution of other bio-materials and biogenic composites [25,28,78].

Many models have been applied to analyze experimental sorption equilibrium data [79]. The optimization of the design of an adsorption system to remove dye from solutions is designed to establish the most appropriate correlation for the equilibrium curve. The adsorption data of MB were fitted according to a Langmuir model [80,81] and are represented in linear form in Eq. (10):

$$\frac{C_e}{q_e} = \frac{C_e}{q_m} + \frac{1}{q_m * K_L} \quad (10)$$

where C_e ($mg{\cdot}L^{-1}$) and q_e ($mg{\cdot}g^{-1}$) are the concentrations of adsorbate in solution and in adsorbent at equilibrium, respectively; q_m is the maximum adsorption capacity ($mg{\cdot}g^{-1}$) and K_L ($L{\cdot}mg^{-1}$) is the Langmuir constant.

The Freundlich isotherm model is an empirical equation that assumes the multilayer adsorption on heterogeneous adsorption sites, and the adsorption capacity is influenced by the adsorbate equilibrium concentration [82]. The equation could be expressed by Eq. (11) [83]:

$$Ln(q_e) = \frac{1}{n} Ln(C_e) + Ln(K_F) \quad (11)$$

where K_F and 1/n represent the Freundlich characteristic constants, suggesting the adsorption capacity and adsorption intensity, respectively.

Figs. 10 and 11 present the curve evolution of the Langmuir and Freundlich models. The correlation coefficients (R^2) of the linear representations of the Langmuir equation are higher than those of the Freundlich equation in both samples. The linearity of the plots for MB adsorbed on TOS, TOS5 and TOS20 (Fig. 10) with R^2 which tends towards 1 has confirmed that the Langmuir model is the adequate choice. In the case of TOS, only the first region of the adsorption isotherms was taken into account since the model applies to monolayer formation. The equilibrium Langmuir constant K_L as well as the maximum amount of adsorbed molecules

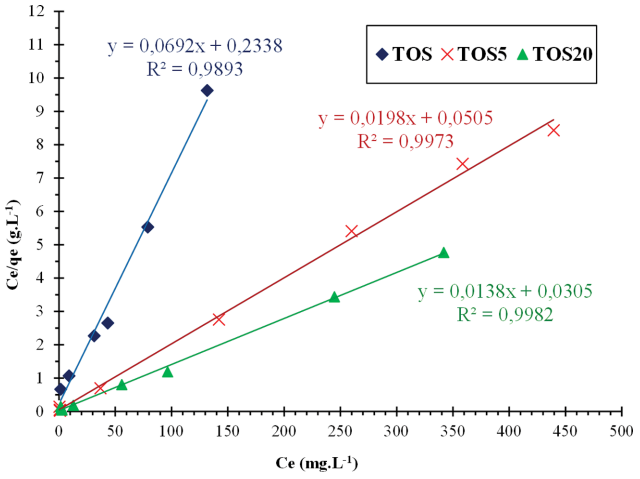

Fig. 10. Transformed Langmuir adsorption isotherms for untreated and treated TOS.

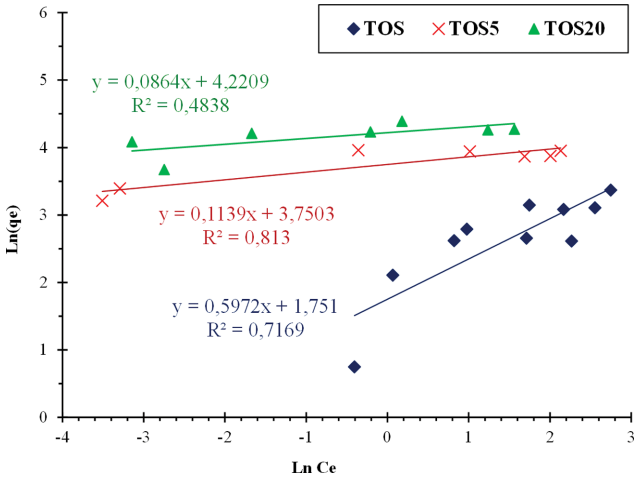

Fig. 11. Transformed Freundlich adsorption isotherms for untreated and treated TOS.

at the cellulose surface, q_m, were calculated and summarized in Table 6. These results suggest the following remarks:

- The q_m values deduced graphically were close to those observed at the plateau in the adsorption isotherms curves, which confirms the validity of the model proposed.

- The adsorption equilibrium constants increased in the order TOS>TOS5>TOS20. In fact, for a concentration of 5% w/v of sodium hydroxide (TOS5), there is a purification treatment by removing impurities (hemicellulose, lignin ...) [83]. By increasing the concentration of NaOH (TOS20), the effect would be more important. There is, in fact, a modification of the crystalline structure of cellulose I to cellulose II for TOS5 to TOS20, respectively. As has been indicated, mercerization induces a decrease in the crystalline zone with the increase in amorphous zones, thus enhancing the accessibility of MB as dye absorbate [84]. This was also confirmed by the progressive decrease in the values of the adsorption free energy ΔG^o calculated using Eq. (12):

$$\Delta G^o = -RT\ LnK \quad (12)$$

where T is the temperature (K), R is universal gas constant (8.314 $J{\cdot}mol^{-1}{\cdot}K^{-1}$), and K ($L{\cdot}mol^{-1}$) is an equilibrium constant defined as the product of the Langmuir constants q_m and K_L.

The negative values of ΔG^o indicate the spontaneous adsorption of MB onto TOS and treated TOS. The absolute values of ΔG^o were less than 20 $KJ{\cdot}mol^{-1}$, which indicates that physi-sorption of MB takes place on both TOS and extracted cellulosic fibers [85,86].

The feasible adsorption mechanism of MB dye onto the surface of cellulosic supports adsorbent might be due to the mechanism shown in Fig. 12. In the alkaline medium of MB, the hydroxyl groups can be deprotonated (Fig. 6). Hence, the surface of cellulosic supports has a negative charge (CO^-) that may interact strongly with cationic MB dye and get adsorbed onto the surface of adsorbent by electrostatics forces of attraction [87]. Likewise, hydrogen bonds are formed between the hydroxyl groups (-OH) of adsorbent and electronegative atom (N and S) of MB dye. Fig. 12 depicts the systematic representation of hydrogen bonding between the

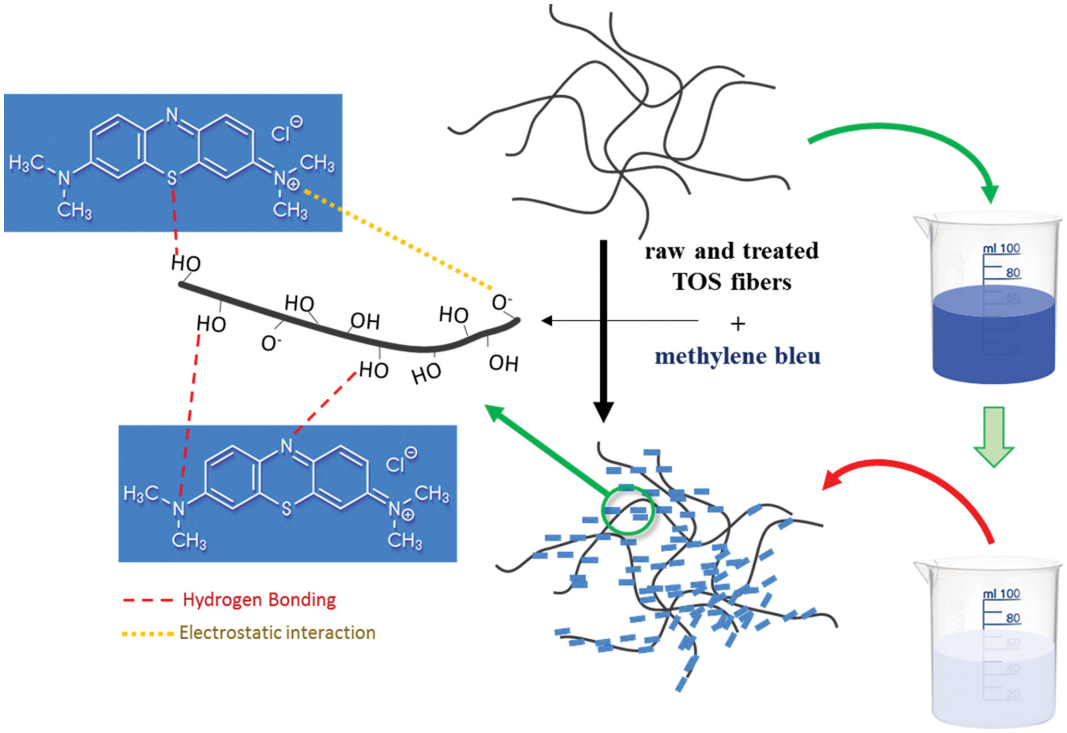

Fig. 12. Mechanism of adsorption of MB dye onto TOS in basic medium.

hydroxyl group and nitrogen and sulfur atoms of MB. As a result, MB dye molecules get adsorbed onto the surface of cellulosic substrates.

6-4. Comparison of Performances

The results of the maximum adsorption capacity of raw and treated TOS fibers towards MB molecules obtained from the Langmuir isotherm model were compared with other reported work listed in Table 7. In our research study, the maximum adsorption capacity values of methylene blue on cellulosic TOS, TOS5, TOS20 supports were 14, 52 and 76 $mg \cdot g^{-1}$, respectively. These results were compared to various adsorbents prepared by other research works. Relatively, a similar study conducted in the same laboratory using softwood sawdust gave a maximum adsorption capacity that was almost equivalent to that of TOS.

Table 7. Comparisons between TOS cellulosic supports and other materials on the removal of MB dye

Adsorbent	Maximum adsorption capacity ($mg \cdot g^{-1}$)	References
TOS	14	Current work
TOS5	52	Current work
TOS20	76	Current work
Softwood sawdust	12.6	[91]
NCC powder	118.0	[88]
Carbon nanotube	59.7	[89]
Clay	6.3	[92]
Activated clay	109.1	[90]
Microcrystalline cellulose	5.0	[93]

The cellulosic supports under study revealed a higher adsorption capacity compared to clay and microcrystalline cellulose. Although the adsorption capacity was lower than that of some other adsorbents reported in the literature (Table 7), such as NCC powder [88], carbon nanotube [89] and activated clay [90], the great advantages of cellulosic supports over these adsorbents were the relatively low cost, the feasibility of regeneration and separation of residues after treatment. Therefore, sawdust was considered as an excellent adsorbent for removing methylene blue dye from the aqueous solution because it is characterized by its high adsorption capacity and ease of regeneration.

7. Methylene Blue Desorption

The study of dye desorption was carried out to investigate the regeneration capacity of a previously used adsorbent. The desorption kinetics experiments were carried out on cellulosic TOS raw following BM adsorption. According to the adsorption kinetic and isotherm studies, 1.5 g of TOS previously saturated with BM was immersed in distilled water, pH=10, with constant stirring at room temperature. Fig. 13 presents the variations of desorption efficiency D (%) of MB dye (Eq. (3)) calculated during the adsorption and desorption, respectively, carried out for three combinations of (pH_{ads}, pH_{des}) at (10, 7), (10, 10) and (10, 2). The examination of these curves reveals that the desorption of MB adhered on TOS, whose maximum desorption percentages were reached after 15 min, was rapid. The desorption efficiency of MB in an acidic medium is favored (37%) and it is very low in a basic (0,4%) or neutral (0,7%) medium. Under acidic conditions, the number of positively charged sites increases on the TOS cellulosic substrates [94]. Thus, the increase of the desorption efficiency of MB dye is probably due to the electrostatic repulsion between positively charged

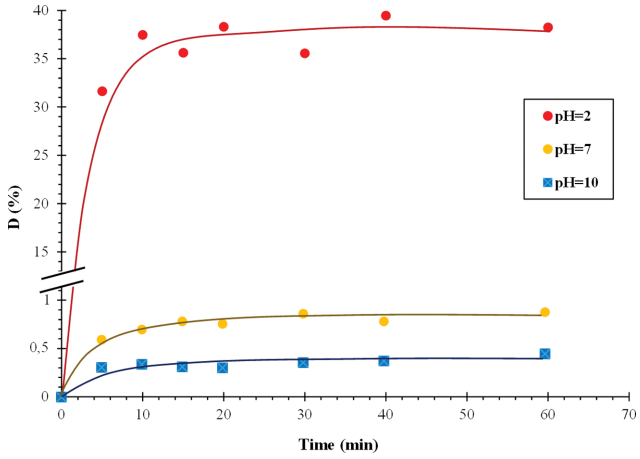

Fig. 13. Variations in desorption efficiency D(%) of MB into TOS by water at different desorption pH : $pH_{dés}$=2, 7 and 10.

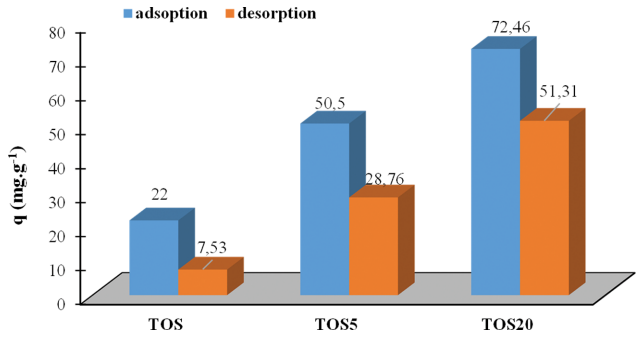

Fig. 14. Variation of the amount adsorbed and desorbed for cellulosic substrates TOS, TOS5 and TOS20.

sites on the TOS surface and cationic dye molecules [94,95]. The histogram of Fig. 14 shows that the desorption of MB adhered on TOS5 and TOS20 by water in acid medium in the first 15 min and using the above protocol even at room temperature was the most effective, with ~57% and 71% of the MB desorbed, respectively.

CONCLUSION

The ability of Tunisian olive sawdust, used as an agro-based waste biomass to the isolation of Cellulose I and II and the adsorption of MB, was investigated. The results proved that the micro-fibrils of olive sawdust underwent a change of assembly and orientation by the conversion of the surface into a swollen and straightened state after the alkali treatment. Thus, the rearrangement from native cellulose I (TOS5) to cellulose II (TOS20) with the increase of NaOH concentration was revealed by XRD and ATR analysis. With 5% of NaOH concentration, the crystallinity index increased by removing hemicellulose and lignin in large part from raw TOS. However, the decrease of crystallinity index of the high concentration with NaOH (20%) is related to the change in the microstructure of cellulosic fibers by the formation of the cellulose structure II. The deconvolution of OH stretching vibration bands of FTIR spectrum confirmed that the transition from cellulose I to cellulose II was achieved by breaking the intramolecular hydrogen bonds and the formation of new intermolecular bonds in the fibrous structure.

The positive impact of the change in crystalline structure by the mercerization process on the degree of accessibility of cellulosic supports isolated from olive sawdust was confirmed by the increased values of ISV analysis. Therefore, the ability of all cellulosic supports in the adsorption of MB was investigated. At room temperature, a basic medium (pH=10,5) favored the adsorption of MB on different cellulosic supports from Tunisian olive sawdust (TOS). The adsorption isotherms of MB on the different cellulosic supports of TOS and the related correlation confirmed that the Langmuir model was the adequate choice. The adsorption equilibrium constants increased with supports after alkaline treatment in the order of TOS (94 $L{\cdot}mol^{-1}$)<TOS5 (125 $L{\cdot}mol^{-1}$)< TOS20 (139 $L{\cdot}mol^{-1}$). The desorption efficiency D in acidic medium of MB increased with ~57% and 71% of the MB desorbed onto TOS 5 and TOS20, respectively. The experimental results show that the adsorption of MB on the raw and alkali treated olive sawdust cellulosic supports was of physical nature, thus allowing reuse of the adsorbed supports. This may lead to an increase in the adsorption capacity of regenerated materials, considered as waste, thus contributing to the fight against water pollution by organic contaminants.

FUNDING

None. No funding to declare.

CONFLICTS OF INTEREST

The authors declare no conflict of interest.

AVAILABILITY OF DATA AND MATERIALS

Authors confirm that all relevant data are included in the article.

CODE AVAILABILITY

Not applicable

SUPPORTING INFORMATION

Additional information as noted in the text. This information is available via the Internet at http://www.springer.com/chemistry/journal/11814.

REFERENCES

1. P. Chowdhary, R. N. Bharagava, S. Mishra and N. Khan, *Environmental Concerns and Sustainable Development*, 235 (2019).
2. S. Gupta, S. B. Pawar and R. A. Pandey, *Sci. Total. Environ.*, **687**, 1107 (2019).
3. S. Keskes, W. Jallouli, E. Sahli, S. Sayadi and S. Tounsi, *Bioresources and Bioprocessing*, **7**, 1 (2020).

4. N. Methneni, R. Anthonissen, J. Van de Maele, F. Trifa, L. Verschaeve, H. B. Mansour and B. Mertens, *Environ. Sci. Pollut. Res.*, **27**, 40088 (2020).
5. F. I. Hai, K. Yamamoto and K. Fukushi, *Crit. Rev. Environ. Sci. Technol.*, **37**, 315 (2007).
6. S. B. Jadhav, S. S. Phugare, P. S. Patil and J. P. Jadhav, *Int. Biodeterior. Biodegradation*, **65**, 733 (2011).
7. B. D. Tripathi and S. C. Shukla, *Environ. Pollut.*, **69**(1), 69 (1991).
8. N. Cao, C. Yue, Z. Lin, W. Li, H. Zhang, J. Pang and Z. Jiang, *J. Hazard. Mater.*, **414**, 125489 (2021).
9. R. S. Juang, W. C. Huang and Y. H. Hsu, *Hazard. Mater.*, **46**, 52 (2009).
10. L. Zhang, P. Lv, Y. He, S. Li, K. Chen and S. Yin, *J. Clean. Prod.*, **273**, 122863 (2020).
11. A. Kuleyin, A. Gök and F. Akbal, *J. Environ. Chem. Eng.*, **9**(1), 104782 (2021).
12. L. Bilińska, K. Blus, M. Foszpańczyk, M. Gmurek and S. Ledakowicz, *J. Environ. Manage.*, **265**, 110502 (2020).
13. H. Khan, A. K. Khalil, A. Khan, K. Saeed and N. Ali, *Korean J. Chem. Eng.*, **33**, 2802 (2016).
14. H. Deng, J. Yin, J. Ma, J. Zhou, L. Zhang, L. Gao and T. Jiao., *Appl. Surf. Sci.*, **543**, 148821 (2021).
15. C. Qian, J. Yin, J. Zhao, X. Li, S. Wang, Z. Bai and T. Jiao, *Coll. Surf. A: Physicochem. Eng. Aspects.*, **610**, 125752 (2021).
16. J. Yin, B. Ge, T. Jiao, Z. Qin, M. Yu, L. Zhang, Q. Zhang and Q. Peng, *Langmuir*, **37**(3), 1267 (2021).
17. S. Babel, *J. Hazard. Mater.*, **97**(1-3), 219 (2003).
18. K. Gul, H. Khan, N. Muhammad, B. Ara and T. U. H. Zia, *Sep. Sci. Technol.*, **56**(15), 2507 (2021).
19. N. Somsesta, C. Piyamawadee, V. Sricharoenchaikul and D. Aht-Ong, *Korean J. Chem. Eng.*, **37**(11), 1999 (2020).
20. Y. S. Raja, M. F. R. Samsudin and S. Sufian, *Arab. J. Sci. Eng.*, **46**, 6349 (2021).
21. A. E. Ofomaja, *Process. Biochem.*, **42**, 16 (2007).
22. F. Banat, S. Al-Asheh, R. Al-Ahmad and F. Bni-Khalid, *Bioresour. Technol.*, **98**(16), 3017 (2007).
23. Y. S. Ho and G. Mckay, *Process. Saf. Environ.*, **76**(2), 183 (1998).
24. I. Bouaziz, M. Hamza, A. Sellami, R. Abdelhedi, A. Savall and K. Groenen Serrano, *Sep. Purif. Technol.*, **175**, 1 (2017).
25. H. Pekkuz, İ. Uzun and F. Güzel, *Bioresour. Technol.*, **99**(6), 2009 (2008).
26. V. C. Taty-Costodes, H. Fauduet, C. Porte and A. Delacroix, *J. Hazard. Mater.*, **105**(1-3), 121 (2003).
27. J. A. Menéndez-Díaz and I. Martín-Gullón, *Interface Sci. Technol.*, **7**, 1 (2006).
28. M. Jaouadi, *Int. Wood Prod. J.*, **12**(1), 22 (2020).
29. A. E. Ofomaja, E. I. Unuabonah and N. A. Oladoja, *Bioresour. Technol.*, **101**(11), 3844 (2010).
30. S. P. Gautam, P. S. Bundela, A. K. Pandey, J. Jamaluddin, M. K. Awasthi and S. Sarsaiya, *J. Appl. Nat. Sci.*, **2**(2), 330 (2010).
31. P. Zugenmaier, *Crystalline cellulose and derivatives*, Springer Series in Wood Science (2008).
32. D. Fengel and G. Wegener, *Wood: chemistry ultrastructure reactions*, Walter de Gruyter, Berlin and New York (1984).
33. P. Zugenmaier, *Prog. Polym. Sci.*, **26**(9), 1337 (2001).
34. A. J. Ragauskas, C. K. Williams, B. H. Davison, G. Britovsek, J. Cairney, C. A. Eckert, W. J. Frederick, J. P. Hallett, D. J. Leak, C. L. Liotta, J. R. Mielenz, R. Murphy, R. Templer and T. Tschaplinski, *Science*, **311**(5760), 484 (2006).
35. S. Y. Oh, D. I. Yoo, Y. Shin, H. C. Kim, H. Y. Kim, Y. S. Chung, W. H. Parkd and J. H. Youke, *Carbohyd. Res.*, **340**(15), 2376 (2005).
36. J. M. Faulstich de Paiva and E. Frollini, *Macromol. Mater. Eng.*, **291**(4), 405 (2006).
37. R. Jinping, T. Furong and C. Yuezhi, *J. Polym. Environ.*, **28**, 1302 (2020).
38. E. C. Osoka and O. D. Onukwuli, *Int. J. Adv. Mater. Res.*, **1**(3), 95 (2015).
39. P. Goswami, R. S. Blackburn, H. M. El-Dessouky, J. Taylor and P. White, *Eur. Polym. J.*, **45**(2), 45 (2009).
40. E. Dinand, M. Vignon, H. Chanzy and L. Heux, *Cellulose*, **9**, 7 (2002).
41. A. E. Oudiani, Y. Chaabouni, S. Msahli and F. Sakli, *Carbohyd. Polym.*, **86**(3), 1221 (2011).
42. A. C. O'sullivan, *Cellulose*, **4**(3), 173 (1997).
43. K. Kayoko, K. Satoshi, T. Eiji and W. Masahisa, *Carbohyd. Polym.*, **83**, 483 (2011).
44. K. E. Borchani, C. Carrot and M. Jaziri, *Cellulose*, **22**(3), 1577 (2015).
45. M. J. John and R. D. Anandjiwala, *Polym. Composite*, **29**(2), 187 (2008).
46. J. Siroky, S. B. Richard, B. Thomas and T. P. W. Jim, *Carbohydr. Polym.*, **84**(1), 299 (2011).
47. V. A. G. Leandro, K. J. Osvaldo, P. F. Rossimiriam and F. G. Laurent, *Bioresour. Technol.*, **99**(8), 3077 (2008).
48. M. L. Nelson and T. Mares, *Text. Res. J.*, **35**(7), 592 (1965).
49. M. L. Nelson, M. A. Rousselle, S. J. Cangemi and P. Trouard, *Text. Res. J.*, **40**(10), 872 (1970).
50. A. E. O. Ben Sghaier, Y. Chaabouni, S. Msahli and F. Sakli, *Ind. Crop. Prod.*, **36**(1), 257 (2012).
51. L. Segal, J. J. Creely, A. E. Martin and C. M. Conrad, *Text. Res. J.*, **29**(10), 786 (1959).
52. Y. Yue, C. Zhou, A. D. French, G. Xia, G. Han, Q. Wang and Q. Wu, *Cellulose*, **19**(4), 1173 (2012).
53. J. Jayaramudu, A. Maity, E. R. Sadiku, B. R. Guduri, A. V. Rajulu, C. V. V. Ramana and R. Li, *Carbohydr. Polym.*, **86**(4), 1623 (2011).
54. H. K. Seong, M. L. Christopher and K. Kabindra, *Korean J. Chem. Eng.*, **30**(12), 2127 (2013).
55. R. Sun, J. M. Lawther and W. B. Banks, *J. Appl. Polym. Sci.*, **62**(9), 1473 (1996).
56. H. A. Krässig, *Cellulose: Structure, accessibility, and reactivity*, Gordon and Breach Sci. Publications, Yverdon, Switzerland (1993).
57. M. L. Nelson and R. T. O'Connor, *J. Appl. Polym. Sci.*, **8**(3), 1325 (1964).
58. S. Y. Oh, D. I. Yoo, Y. Shin and G. Seo, *Carbohyd. Res.*, **340(3)**, 417 (2005).
59. M. L. Nelson and R. T. O'Connor, *J. Appl. Polym. Sci.*, **8**(3), 1311 (1964).
60. C. Y. Liang and R. H. Marchessault, *J. Polym. Sci.*, **39**, 269 (1959).
61. X. Colom, and F. Carrillo, *Eur. Polym. J.*, **38**(11), 2225 (2002).
62. J. J. Cael, K. H. Gardner, J. L. Koenig and J. Blackwell, *J. Chem. Phys.*, **62**, 1145 (1975).
63. M. A. Clemens, H. T. Lynne, N. F. Anwesha and C. J Michael, *Biomacromolecules*, **15**(3), 791 (2014).

64. T. Kondo, *Cellulose*, **4**, 281 (1997).
65. M. Schwanninger, J. C. Rodrigues, H. Pereira and B. Hinterstoisser, *Vibrat. Spectrosc.*, **36**(1), 23 (2004).
66. D. Fengel and C. Strobel, *Acta. Polymerica*, **45**(4), 319 (1994).
67. A. El Oudiani, Y. Chaabouni, S. Msahli and F. Sakli, *Carbohy. Polym.*, **86**(3), 1221 (2011).
68. R. HAtalla and D. L. Vander Hartb, *Solid. State. Nuclear. Magnetic. Resonance*, **15**(1), 1 (1999).
69. K. Kamide, K. Okjima, T. Matsui and K. Kowsaka, *Polymer. J.*, **16**, 857 (1984).
70. B. Philipp, J. Kunze and H. P. Fink, *Am. Chem. Soc. Symp. Ser.*, **340**, 178 (1987).
71. K. H. Meyer and L. Misch, *Chim. Acta*, **20**(1), 232 (1937).
72. B. Levent, S. Murat, S. Mehmet and Y. Mithat, *Arab. J. Sci. Eng.*, **45**, 7429 (2020).
73. P. K. Gupta, V. Uniyal and S. Naithani, *Carbohyd. Polym.*, **94**(2), 843 (2013).
74. O. Hamdaoui, *J. Hazard. Mater. B.*, **135**(1-3), 264 (2006).
75. S. Langergren and B. K. Svenska, *Handlingar*, **24**, 1 (1898).
76. Y. S. Ho and G. Mckay, *Can. J. Chem. Eng.*, **76**(4), 822 (1998).
77. Y. S. Ho and G. McKay, *Process. Biochem.*, **34**, 451 (1999).
78. M. H. Beyki, M. Bayat, S. Miri, F. Shemirani and H. Alijani, *Ind. Eng. Chem. Res.*, **53**(39), 14904 (2014).
79. C. Tien, Newton, Boston, USA: Butterworth-Heinemann (1994).
80. I. Langmuir, *J. Am. Chem. Soc.*, **38**(11), 2221 (1916).
81. I. Langmuir, *J. Am. Chem. Soc.*, **40**(9), 1361 (1918).
82. A. Mittal, A. Malviya, D. Kaur, J. Mittal and L. Kurup, *J. Hazard. Mater.*, **148**(1-2), 229 (2007).
83. H. M. F. Freundlich, *J. Phys. Chem. A*, **57**, 385 (1906).
84. L. Y. Mwaikambo and M. P. Ansell, *J. Appl. Polym. Sci.*, **84**(12), 2222 (2002).
85. Y. Yu, Y. Y. Zhuang and Z. H. Wang, *J. Colloid Interface Sci.*, **242**(2), 288 (2001).
86. M. T. Yagub, T. K. Sen, S. Afroze and H. M. Ang, *Adv. Colloid Interface Sci.*, **209**, 172 (2014).
87. M. Boumediene, H. Benaïssa, B. George, St. Molina and A. Merlin, *J. Mater. Environ. Sci.*, **9**(6), 1700 (2018).
88. R. Batmaz, N. Mohammed, M. Zaman, G. Minhas, R. M. Berry and K. C. Tam, *Cellulose*, **21**(3), 1655 (2014).
89. S. Wang, C. W. Ng, W. Wang, Q. Li and Z. Hao, *Chem. Eng. Technol.*, **197**, 34 (2012).
90. C. H. Weng and Y. F. Pan, *J. Hazard. Mater.*, **144**(1-2), 355 (2007).
91. I. Bouaziz, C. Chiron, R. Abdelhedi, A. Savall and K. Groenen Serrano, *Environ. Sci. Pollut. R.*, **21**(14), 8565 (2014).
92. A. Gürses, S. Karaca, Ç. Doğar, R. Bayrak, M. Açıkyıldız and M. Yalçın, *J. Colloid Interface Sci.*, **269**(2), 310 (2004).
93. K. B. Tan, A. Z. Abdullah, B. A. Horri and B. Salamatinia, *J. Chem. Soc. Pak.*, **38**(4), 651 (2016).
94. K. Vijayaraghavan, M. W. Lee and Y. S. Yun, *Bioresour. Technol.*, **99**, 5778 (2008).
95. R. Abdallah and S. Taha, *Chem. Eng. J.*, **195**, 69 (2012).

Supporting Information

Isolation, characterization and methylene blue adsorption: Application of cellulose from olive sawdust

Fatma. Njeh*, Morched. Hamza*, Ines. Bouaziz*, Ridha. Abdelhedi*, and Makki. Abdelmouleh,†**

*Laboratory of Electrochemistry and Environment (LEE), Sfax National Engineering School (ENIS) BPW, 3038 Sfax, University of Sfax, Tunisia
**Laboratory of Material Science and Environment (LMSE)-Faculty of Science of Sfax (University of Sfax) 3038 Sfax-Tunisia
(*Received 27 April 2021 • Revised 19 July 2021 • Accepted 15 August 2021*)

FTIR Analysis

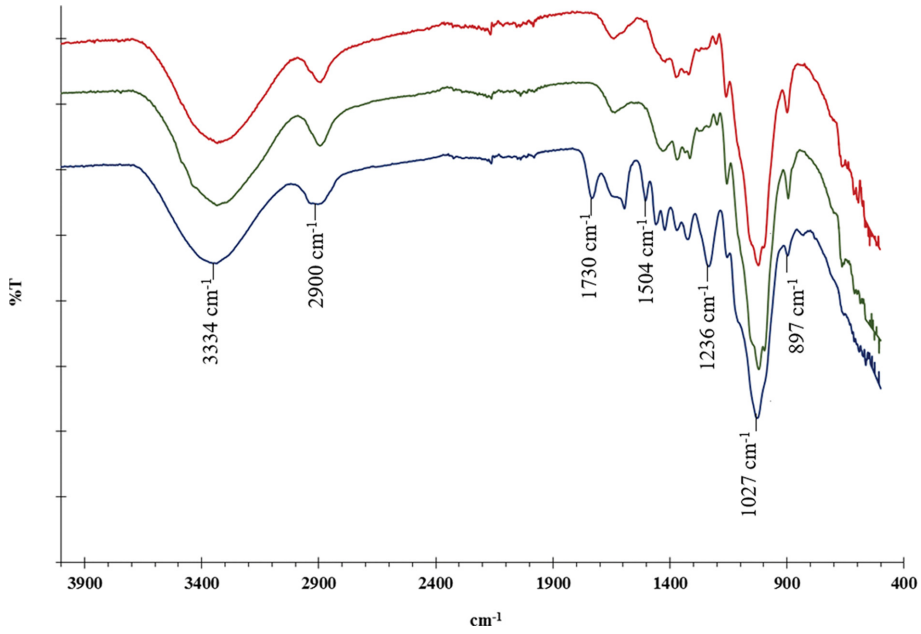

Fig. S1. FTIR Spectrum of untreated TOS (blue) and treated TOS: TOS5 (green) and TOS20 (red).

Thermogravimetric Analysis

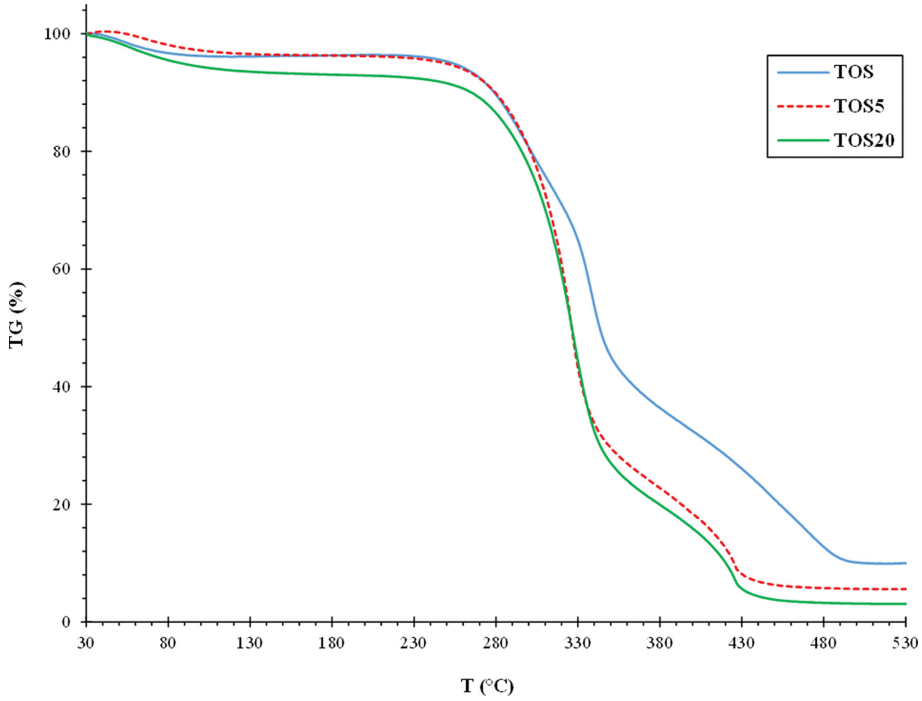

Fig. S2. TG curves of TOS, TOS5 and TOS20.